AIMS Mathematics, 9(7): 18013–18033.
DOI: 10.3934/math.2024878
Received: 20 March 2024
Revised: 01 May 2024
Accepted: 09 May 2024
Published: 27 May 2024

https://www.aimspress.com/journal/Math

Research article

Lie symmetry analysis, and traveling wave patterns arising the model of transmission lines

Adil Jhangeer[1,2,*], Ali R Ansari[3], Mudassar Imran[4], Beenish[5] and Muhammad Bilal Riaz[1,6]

[1] IT4Innovations, VSB–Technical University of Ostrava, Ostrava-Poruba, Czech Republic; muhammad.bilal.riaz@vsb.cz
[2] Department of Mathematics, Namal University, 30KM Talagang Road, Mianwali 42250, Pakistan;
[3] Centre for Applied Mathematics and Bioinformatics (CAMB), Gulf University for Science and Technology, Kuwait; ansari.a@gust.edu.kw
[4] College of Humanities and Sciences, Ajman University, Ajman, UAE; mudassar.Imran@ajman.ac.ae
[5] Department of Mathematics, Quaid-I-Azam University 45320, Islamabad, Pakistan; beenishmasood2141@gmail.com
[6] Department of Computer Science and Mathematics, Lebanese American University, Byblos, Lebanon

* **Correspondence:** Email: adil.jhangeer@vsb.cz.

Abstract: This work studies the behavior of electrical signals in resonant tunneling diodes through the application of the Lonngren wave equation. Utilizing the method of Lie symmetries, we have identified optimal systems and found symmetry reductions; we have also found soliton wave solutions by applying the tanh technique. The bifurcation and Galilean transformation are found to determine the model implications and convert the system into a planar dynamical system. In this experiment, the equilibrium state, sensitivity, and chaos are investigated and numerical simulations are conducted to show how the frequency and amplitude of alterations affect the system. Furthermore, local conservation rules are demonstrated in more detail to unveil the whole system of movements.

Keywords: Lonngren wave equation; bifurcation analysis; sensitivity analysis; Lyapunov exponent; multistability analysis; Lie point symmetry
Mathematics Subject Classification: 22E60, 35C07, 35Q60

1. Introduction

The transmission line in this investigation is similar to one that was previously used to examine

solitary waves. Figure 1 illustrates a segment of the 50-section line. Each section comprises a parallel resonant circuit with a resonance frequency of $\frac{v_0}{2m} \sim 30$ MHz in the series Additionally, there is a reverse-biased $p-m$ junction diode in the shunt branch, and its capacitance varies based on the bias and signal voltages. The entire length of the line spans 100 cm. The voltage variable W, can be established by using transmission line equations [1]:

$$\begin{cases} \dfrac{\partial J}{\partial \varpi} + \dfrac{\partial [WD_n(W)]}{\partial \iota} = 0, \\ \dfrac{\partial W}{\partial \varpi} + L\dfrac{\partial J'}{\partial \iota} = 0, \\ \dfrac{\partial^2 W}{\partial \varpi \partial \iota} + \dfrac{1}{S}(J - J') = 0. \end{cases} \tag{1.1}$$

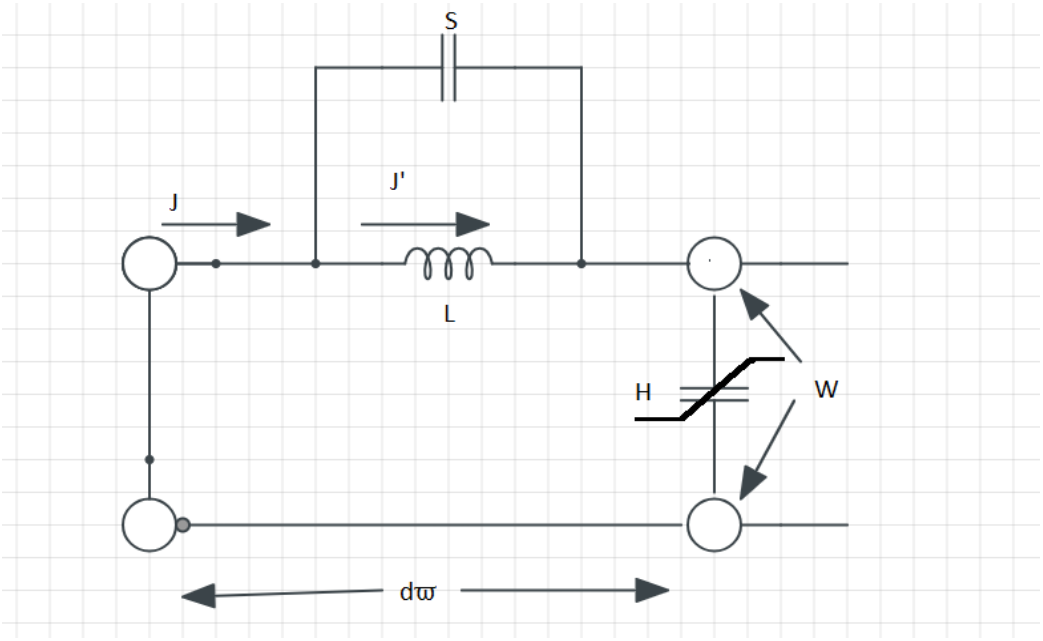

Figure 1. The nonlinear dispersive transmitting line's characteristic section.

The quantities L and $\frac{1}{S}$ have units expressed in henry per unit length and $(\frac{1}{farads})$ per unit length respectively. The nonlinear diode is denoted by $H = D_n(W)$. By utilizing the given information, we can formulate Eq (1.1) by describing the voltage W as a wave equation:

$$\frac{\partial^4 W}{\partial \varpi^2 \partial \iota^2} + \frac{1}{LD_s}\frac{\partial^2 W}{\partial \varpi^2} - \frac{1}{D_s}\frac{\partial^2 (WH)}{\partial \iota^2} = 0. \tag{1.2}$$

We can confidently state that $D_n(W)$ is equivalent to $D_{n_0}(\frac{W}{\overline{W}})^{-m}$. Here, $\overline{W}$ represents a normalizing constant, and m is a numerical value. Our analysis will demonstrate that $0 < m < 1$, which encompasses various potential experimental values (in our experiments, $m = \frac{1}{3}$). Incorporating dimensionless units into Eq (1.2) transforms it into the following non-linear 4^{th}-order partial differential equation (PDE) through the use of the nonlinear (spiral) group:

$$\frac{\partial^4 Q}{\partial \iota^2\, \partial \varpi^2} - a\frac{\partial^2 Q}{\partial \iota^2} + \frac{\partial^2 Q}{\partial \varpi^2} + 2b\Big[(\frac{\partial Q}{\partial \iota})^2 + Q\frac{\partial^2 Q}{\partial \iota^2}\Big] = 0. \tag{1.3}$$

Equation (1.3) represents the Lonngren wave equation [2], which holds great significance and has been garnering attention as a captivating mathematical model owing to its extensive applications in the field of electrical science. This study is based on the use of the Lonngren wave equation which is a potent numerical technique that helps to model the electrical signals of tunnel diodes. Although it was developed to reproduce wave propagation in shallow water, the equation may now, also be used to interpret electrical pulses in a telegraphic system with the use of tunnel diodes. It can be applied as both a research subject and an object of scientific study. We will explore the role of arbitrary constants a and b, along with the spatial variable ϖ and the temporal variable ι, in the representation of the wave function $Q(\varpi, \iota)$. The relationship between Q and its components will be thoroughly examined in our discussion. The constant b also acts as a coefficient to demonstrate the nonlinearity of Eq (1.3). The mathematical focus for this equation is the behavior of electrical impulses in Sony's tunnel diode, which is a type of semiconductor diode [3]. Equation (1.3) may also be used to clarify how energy is stored in circuits with an electric charge or the way electrical signals, are transferred via materials with semiconductor properties [4].

In previous studies, Lonngren et al. [3] utilized a non-linear differential equation to describe a certain physical phenomenon, while Akçağı and Aydemir [5] explored the connection between their approaches by employing the $(\frac{G'}{G})$ expansion method and the modified extended tanh method. These studies shed light on the understanding and analysis of such an intriguing phenomenon, which will be further examined in our discussion. Baskonus et al. [6] created novel complex hyperbolic constructions by employing the sine-Gordon expansion method. Zhang et al. [2] identify traveling wave solutions, which we classify as trigonometric, and rational by employing $exp(-\psi(\eta))$ expansion function technique.

Mathematical techniques are of great importance in the development of models that reflect functions within different disciplines like physics [7], chemistry [8], and epidemiology [9]. The phenomenon of ever-increasing scientific community interest in solving nonlinear PDEs (NLPDEs) is in turn a trend in the modeling of various phenomena for which these equations are applied. This increasing interest demonstrates the growing significance and relevancy of these equations; thus, researchers, in turn, continue to further their conduct of a thorough treatment and explore their consequences [10]. The scientific community is actively engaged in researching the physical interpretation of these solutions of the NLPDE, as highlighted by Baskonus and Bulut [11]. Numerous NLPDEs, such as the Riemann wave equation in fluid dynamics [7], Boltzmann equation in statistical mechanics [12], Fitzhugh-Nagumo equation in biological neuron models [13], and Kadomtsev-Petviashvili equation in shallow water waves [14], contribute to the understanding and application of these models for various physical phenomena. The solutions derived in these studies are commonly referred to as soliton solutions [15], a concept initially introduced by Russell [16] following observations of water waves.

The concept of a soliton, as described by Drazin and Johnson [17], is based on possessing three significant characteristics. First, a soliton is characterized as a wave that travels consistently without any alteration in its wave behavior. Second, solitons possess the ability to interact with other solitons. Solitons are known to be confined to specific regions, and oceanic optic soliton technology has become an important asset in the smooth transmission of information. Nowadays, the existence of several electronic channels such as social networking sites, Facebook posts, Twitter comments, and so on owes much to the soliton technology. Our phenomenon refers to a pulse that maintains its shape while traveling at a constant velocity.

The main impetus of the soliton technology research is certainly the significant scientific applications. Different models for studying and explaining the details that have been also constructed. Nonlinear models are preeminent, as they use nonlinear differential equations to describe the behavior of solitons. As researchers continue to employ these equations, there is a proportional increase in the number of solutions that can be computed; also, the hidden secrets of the solitons are further revealed. The findings of this research reach beyond the conventional boundaries of the specialized disciplines, which are now able to employ soliton technology as a key tool across different fields of science and engineering. Mathematical physics attaches great importance to wave patterns as the most fundamental tool for the explanation and prediction of various phenomena. Nevertheless, the quest for exact analytical solutions of nonlinear models is expansive, as such problems have their natural complexities that are not so easy to handle. However, such difficulties do not stop scientists who are interested in these problems due to the relevance they are deepening as a branch of science.

Researchers have dedicated their efforts to nonlinear components, devising and employing various mathematical techniques to generate novel analytical solutions for nonlinear differential equations. These techniques include the extended direct algebraic method [18, 19], new extended auxiliary equation method [20], tanh-coth function method [21], sine-cosine technique [22], generalized Kardashev method [23], exp-function method [24], new Jacobi elliptic functions method [25], and tan-coth method [26]. These analytical methods have proven to be considerably more reliable and efficient when it comes to solving PDEs. In recent times, many researchers have utilized Lie analysis to derive analytical solutions for various nonlinear models. Notable contributions in this regard have been made by scholars such as Jhangeer et al. [27], Hussain et al. [28], and Dorodnitsyn et al. [29]. The literature presents a wide range of solutions, including soliton solutions, trigonometric solutions, lump wave solutions, and more [30, 31]. Solitons, which are waves that maintain their shape while moving at a constant speed, are particularly interesting in the context of optical solitons. Several nonlinear models have soliton solutions, including the Noyes field model [32], Boussinesq equation [33], and sine-Gordon equation [34].

The conservation laws play a fairly important role in dynamic systems of all kinds, and they may be used across disciplines. They are indispensable in the study of numerous phenomena, ranging from the physical properties of PDEs that model various processes and interactions to the other phenomena. They are applied for the discovery of integrability and linearization of PDEs, detection of first integrals for ordinary differential equations, determination of the potentials, formation of non-locally connected systems, and verification of numerically computed solutions [35, 36]. The fact that various researchers have developed different ways to derive conservation laws is a testament to their significance in computing conserved quantities, which is the ultimate issue of mathematicians and physicists.

This paper is organized as follows. Section 2 presents preliminary details. Section 3 discusses the reduction of symmetries and the construction of traveling wave patterns, as well as presents the graphical results. In Section 4, we detail a bifurcation analysis of the proposed model. Hamiltonian dynamics is utilized in Section 5 to classify the obtained equilibrium points. Section 6 focuses on the analysis of quasiperiodic and chaotic behaviors, which is accompanied by corresponding phase portraits. The Lyapunov characteristic exponent is examined in Section 7 to assess the chaotic behavior of the model. Detailed sensitivity analysis under the initial conditions is presented in Section 8, followed by a multistability analysis in Section 9. Additionally, in Section 10, we detail the use of the multiplier method to derive a comprehensive set of conservation laws for Eq (1.2). Finally, the

results of the study are summarized in the conclusion in Section 11.

2. Lie symmetry analysis

A one-parameter Lie group with infinitesimal transformation is depicted [37]:

$$W = \alpha(\varpi, \iota, Q)\frac{\partial}{\partial \varpi} + \beta(\varpi, \iota, Q)\frac{\partial}{\partial \iota} + \gamma(\varpi, \iota, Q)\frac{\partial}{\partial Q}, \tag{2.1}$$

where the infinitesimal generators are $\alpha(\varpi, \iota, Q), \beta(\varpi, \iota, Q)$ and $\gamma(\varpi, \iota, Q)$.

By imposing certain symmetry conditions, a symmetry for Eq (1.3) can be achieved for the vector field associated with Eq (2.1):

$$\begin{cases} Pr^{[4]}W(\sigma)|_{\sigma=0} = 0, \\ Pr^{[4]}W = W + \gamma^{\iota}(\varpi, \iota, Q)\dfrac{\partial}{\partial Q_{\iota}} + \gamma^{\varpi\varpi}(\varpi, \iota, Q)\dfrac{\partial}{\partial Q_{\varpi\varpi}} + \gamma^{\mu}(\varpi, \iota, Q)\dfrac{\partial}{\partial Q_{\mu}} + \gamma^{\mu\varpi\varpi}(\varpi, \iota, Q)\dfrac{\partial}{\partial Q_{\mu\varpi\varpi}}, \\ \gamma^{m}_{j_1, j_2, \ldots, j_m} = D_{j_i}(\gamma^{m-1}_{j_1, j_2, \ldots, j_{m-1}}) - (D_{j_m}\alpha^{i})Q_{j_1, j_2, \ldots, j_{m-1}i}, \quad j_i = 1, 2, 3, \ldots, n, \quad \text{for} \quad i = 1, 2, \ldots, m, \\ \quad \text{with} \quad j_1, j_2, \ldots, j_m = \{\varpi, \iota\}, \quad m = 2, 3, 4, \\ \sigma = \dfrac{\partial^4 Q}{\partial \iota^2 \partial \varpi^2} - a\dfrac{\partial^2 Q}{\partial \iota^2} + \dfrac{\partial^2 Q}{\partial \varpi^2} + 2b\left[\left(\dfrac{\partial Q}{\partial \iota}\right)^2 + Q\dfrac{\partial^2 Q}{\partial \iota^2}\right]. \end{cases} \tag{2.2}$$

Regarding ϖ and ι, D_{j_i} $(m = 1, 2, 3, 4)$ is a total operator.

Theorem 1.

Three generators constitute the three-dimensional Lie algebra in Eq (1.3):

$$W_1 = \frac{\partial}{\partial \iota}, \quad W_2 = \frac{\partial}{\partial \varpi}, \quad W_3 = (-2bQ + a)\frac{\partial}{\partial Q} + b\varpi\frac{\partial}{\partial \varpi}.$$

By implementing into consideration Theorem 1, the associated ordinary differential equations, and the initial assumptions, we have:

$$\begin{aligned} \frac{d\bar{\varpi}}{d\zeta} &= \alpha(\bar{\varpi}, \bar{\iota}, \bar{Q}), \ with \quad \bar{\varpi}|_{\zeta=0} = \varpi, \\ \frac{d\bar{\iota}}{d\zeta} &= \beta(\bar{\varpi}, \bar{\iota}, \bar{Q}), \ with \quad \bar{\iota}|_{\zeta=0} = \iota, \\ \frac{d\bar{Q}}{d\zeta} &= \gamma(\bar{\varpi}, \bar{\iota}, \bar{Q}), \ with \quad \bar{Q}|_{\zeta=0} = Q. \end{aligned} \tag{2.3}$$

Using W_j, we have the following one-parameter groups H_j:

$$\begin{aligned} H_1 &: (\varpi, \iota, Q) \rightarrow (\varpi, \iota + \zeta, Q), \\ H_2 &: (\varpi, \iota, Q) \rightarrow (\varpi + \zeta, \iota, Q), \\ H_3 &: (\varpi, \iota, Q) \rightarrow (\varpi e^{b\zeta}, \iota, (Q - \frac{a}{2b})e^{-2b\zeta} + \frac{a}{2b}). \end{aligned} \tag{2.4}$$

Subsequently, the following outcome is derived.

Theorem 2.

Suppose that $Q(\varpi, \iota)$ represents a solution to Eq (1.3); then, there exists an additional solution that is expressed as follows:

$$\begin{aligned} H_1 : (\varpi, \iota) =& (\varpi, \iota - \zeta), H_2 : (\varpi, \iota) = (\varpi - \zeta, \iota), \\ H_3 : (\varpi, \iota) =& [Q(\varpi e^{-b\zeta}, \iota) - \frac{a}{2b}]e^{2b\zeta} + \frac{a}{2b}. \end{aligned} \tag{2.5}$$

Utilizing the definition of the Lie bracket, denoted by $[W_x, W_y] = W_x W_y - W_y W_x$, the commutators can be expressed as follows:

$$\begin{aligned} [W_1, W_1] =& [W_2, W_2] = [W_3, W_3] = 0, \\ [W_1, W_2] =& -[W_2, W_1] = 0, \\ [W_1, W_3] =& -[W_3, W_1] = 0, \\ [W_2, W_3] =& -[W_3, W_2] = bW_2. \end{aligned} \tag{2.6}$$

Theorem 3.

Theorem 1 allows for the formation of a three-dimensional symmetry Lie algebra H through the application of W_j (where j = 1, 2, 3).

In the subsequent step, we aim to find the adjoint representations of the vector fields by using the following Lie series as a basis for our search:

$$Ad_{exp_{(\zeta W_j)}}(W_i) = W_j - \zeta[W_j, W_i] + (\frac{1}{2})[W_j, [W_j, W_i]] - .... \text{ for } \zeta \in \mathbb{R}.$$

By employing the system given by Eq (2.6), we subsequently obtain:

$$\begin{aligned} &Ad_{exp_{(\zeta W_j)}}(W_j) = W_j + O(\zeta^2), \quad j = 1, 2, 3. \\ &Ad_{exp_{(\zeta W_1)}}(W_2) = W_2 + O(\zeta^2), \qquad Ad_{exp_{(\zeta W_2)}}(W_1) = W_1 + O(\zeta^2), \\ &Ad_{exp_{(\zeta W_3)}}(W_1) = W_1 + O(\zeta^2), \qquad Ad_{exp_{(\zeta W_1)}}(W_3) = W_3 + O(\zeta^2), \\ &Ad_{exp_{(\zeta W_2)}}(W_3) = W_3 - \zeta b W_2 + O(\zeta^2), \qquad Ad_{exp_{(\zeta W_3)}}(W_2) = W_2 + \zeta b W_2 + O(\zeta^2). \end{aligned} \tag{2.7}$$

The optimal systems can be derived from the adjoint representations defined in Eq (2.7) as follows.

Theorem 4.

We can derive a one-parameter optimal system by mapping the operators $\{W_1, W_2, W_3, \Delta_1 W_1 + \Delta_2 W_2, \Delta_3 W_1 + \Delta_4 W_3\}$ to the Lie algebra G, where $\Delta_1, \Delta_2, \Delta_3, \Delta_4$ denote arbitrary constants.

3. Reducing symmetries and travelling wave patterns

The subsequent analysis focuses on examining the symmetry reductions and precise solutions for Eq (1.3).

3.1. Reduction by W_1

The generator W_1 yields

$$Q = g(\epsilon_1), \quad \epsilon_1 = \iota. \tag{3.1}$$

Upon substituting Eq (3.1) into Eq (1.3), we obtain an ordinary differential equation represented by

$$-a(\frac{dg}{d\epsilon_1}) + 2b[(\frac{dg}{d\epsilon_1})^2 + g(\frac{d^2g}{d\epsilon_1^2})] = 0.$$

3.2. Reduction by W_2

The generator W_2 yields

$$Q = g(\epsilon_2), \quad \epsilon_2 = \varpi. \tag{3.2}$$

Substituting Eq (3.2) into Eq (1.3) yields a trivial result.

3.3. Dynamical wave solutions

We will introduce the following wave transformation to simplify the scenario as a first step towards solving the problem:

$$Q = G(\epsilon), \quad \epsilon = k(c\iota - \varpi). \tag{3.3}$$

After substituting Eq (3.3) into Eq (1.3), we get the non-linear ordinary differential equation represented by

$$k^4c^2(\frac{d^2G}{d\epsilon^2}) + k^4c^2(\frac{bG^2}{k^2} - \frac{aG}{k^2} + \frac{G}{k^2c^2}) = 0. \tag{3.4}$$

In the following analysis, we will employ the tanh technique to derive a soliton solution for the ordinary differential equation-based Lonngren wave equation, as follows [38]:

$$G(\epsilon) = b_0 + \sum_{i_1=1}^{B} b_{i_1}P^{i_1}, \quad b_B \neq 0. \tag{3.5}$$

To determine the index B, we will compare the highest-order nonlinear term G^2 with the highest-order linear term G'', which yields the value $B = 2$. Consequently, the equation takes the following form:

$$G(\epsilon) = b_0 + b_1P + b_2P^2, \quad b_2 \neq 0. \tag{3.6}$$

By substituting Eq (3.6) into Eq (3.4), we can derive an equation expressed in terms of the powers of P. By organizing the coefficients of similar powers of P, we can establish a set of algebraic equations. After computation using Maple, we can acquire the resultant solutions for Eq (1.3):

Family 1:

$$b_0 = \frac{-1 + (8k^2 + a)c^2}{2bc^2}, \quad b_1 = 0, \quad k = k, \quad b_2 = \frac{-6k^2}{b},$$

$$Q(\varpi, \iota) = \frac{-1 + (8k^2 + a)c^2}{2bc^2} - \frac{6k^2}{b}(tanh(k(c\iota - \varpi)))^2. \tag{3.7}$$

3.4. Graphical behavior

In this section, we present visual representations of the obtained solutions. By choosing suitable parameter values, we were able to derive both two-dimensional and three-dimensional graphical interpretations of Eq (1.3) with $k = 1$, $a = 1$, $b = 1$, and $c = 1$, as shown in Figures 2 and 3. For $k > 0$, the solution exhibits an anti-kink shape.

Similarly, by employing appropriate parameter values, we were able to derive the two-dimensional and three-dimensional graphical representations of Eq (1.3) with $k = -1$, $a = 1$, $b = 1$, and $c = 1$, as shown in Figures 4 and 5. For $k < 0$, the solution takes on a kink shape.

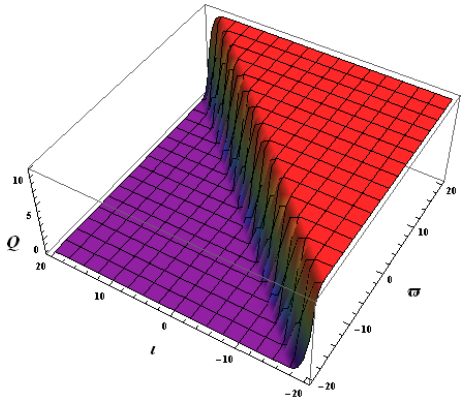

Figure 2. 3D graphics.

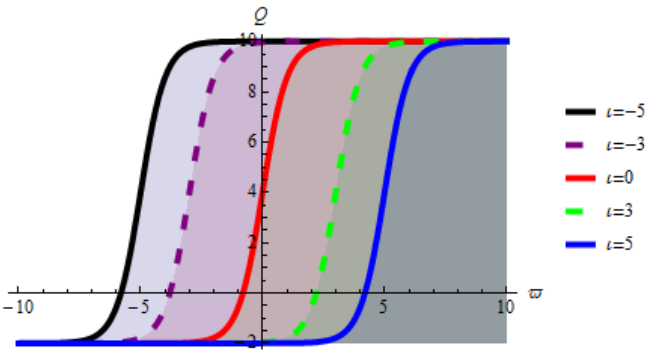

Figure 3. 2D graphics.

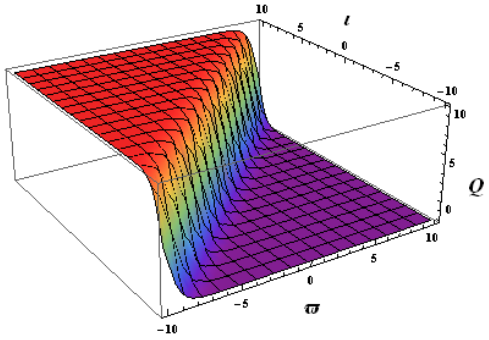

Figure 4. 3D graphics.

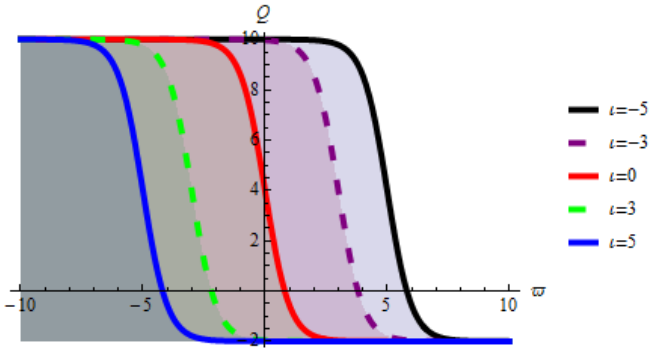

Figure 5. 2D graphics.

4. Bifurcation analysis

Here, we detail the construction of the system of equations shown below through the application of the Galilean transformation to the constructed ordinary differential equation in Eq (3.4):

$$\begin{cases} \dfrac{dG}{d\epsilon} = S, \\ \dfrac{dS}{d\epsilon} = \Omega_1 G - \Omega_2 G^2, \end{cases} \tag{4.1}$$

where $\Omega_1 = (\frac{a}{k^2} - \frac{1}{k^2c^2}), \Omega_2 = \frac{b}{k^2}$. The objective in this scenario is to carry out a thorough bifurcation analysis, which involves looking at phase portraits for the system described by Eq (4.1). We can generate the following system by using Eq (4.1):

$$\begin{cases} S = 0, \\ \Omega_1 G - \Omega_2 G^2 = 0. \end{cases}$$

The equilibrium points that have been identified are:

$$Q_1 = (0, 0), \quad Q_2 = (\frac{\Omega_1}{\Omega_2}, 0).$$

The Jacobian matrix of the system given by Eq (4.1) establishes that

$$J(G, S) = \begin{vmatrix} 0 & 1 \\ \Omega_1 - 2\Omega_2 G & 0 \end{vmatrix}$$

$$= 2\Omega_2 G - \Omega_1.$$

According to the principles of planar dynamical systems, the following statements are true
(1) The center point is located at (G, S) if $J(G, S) > 0$.
(2) The saddle point is located at (G, S) if $J(G, S) < 0$.
(3) The cusp point is located at (G, S) if $J(G, S) = 0$.
In what follows, we present the possible results that may be generated by altering the appropriate parameters:

Category 1: $\Omega_1 > 0$, and $\Omega_2 > 0$.

In Figure 6a, for $a = 2$, $b = 1$, $c = 1$, and $k = 1$, the system has two fixed points: $Q_{1a} = (0, 0)$ and $Q_{2a} = (1, 0)$. It follows that

$$J(Q_{1a}) = -1 < 0, \ J(Q_{2a}) = 1 > 0.$$

Here, Q_{1a} acts as a saddle point, while Q_{2a} serves as a center point. These specific points are depicted in Figure 6a. Nonlinear periodic trajectory structures can be computed by using the Runge-Kutta method, and they are illustrated in Figure 6a.

Category 2: $\Omega_1 > 0$, and $\Omega_2 < 0$.

In Figure 6b, for $a = 2$, $b = -1$, $c = 1$, and $k = 1$, the system has two fixed points: $Q_{1b} = (0, 0)$ and $Q_{2b} = (-1, 0)$. It follows that

$$J(Q_{1b}) = -1 < 0, \ J(Q_{2b}) = 1 > 0.$$

Here, Q_{1b} functions as a saddle point, while Q_{2b} acts as a center point. These specific points are shown in Figure 6b. The Runge-Kutta method can be employed to compute structures of nonlinear periodic trajectories, as illustrated in Figure 6b.

Category 3: $\Omega_1 < 0$, and $\Omega_2 > 0$.

In Figure 6c, for $a = -0.1$, $b = 1$, $c = 1$, and $k = 1$, the system has two fixed points: $Q_{1c} = (0, 0)$ and $Q_{2c} = (-1.1, 0)$. It follows that

$$J(Q_{1c}) = 1.1 > 0, \ J(Q_{2c}) = -1.1 < 0.$$

Here, Q_{1c} acts as a center point, while Q_{2c} functions as a saddle point. These specific points are depicted in Figure 6c. Nonlinear periodic trajectory structures can be computed by using the Runge-Kutta method, as illustrated in Figure 6c.

Category 4: $\Omega_1 < 0$, and $\Omega_2 < 0$.

In Figure 6d, for $a = -0.1$, $b = -1$, $c = 1$, and $k = 1$, the system has two fixed points: $Q_{1d} = (0, 0)$ and $Q_{2d} = (1.1, 0)$. It follows that

$$J(Q_{1d}) = 1.1 \ > \ 0, \ J(Q_{2d}) = -1.1 \ < \ 0.$$

Here, Q_{1d} functions as a center point, while Q_{2d} acts as a saddle point. These specific points are shown in Figure 6d. The Runge-Kutta method can be employed to compute structures of nonlinear periodic trajectories, as illustrated in Figure 6d.

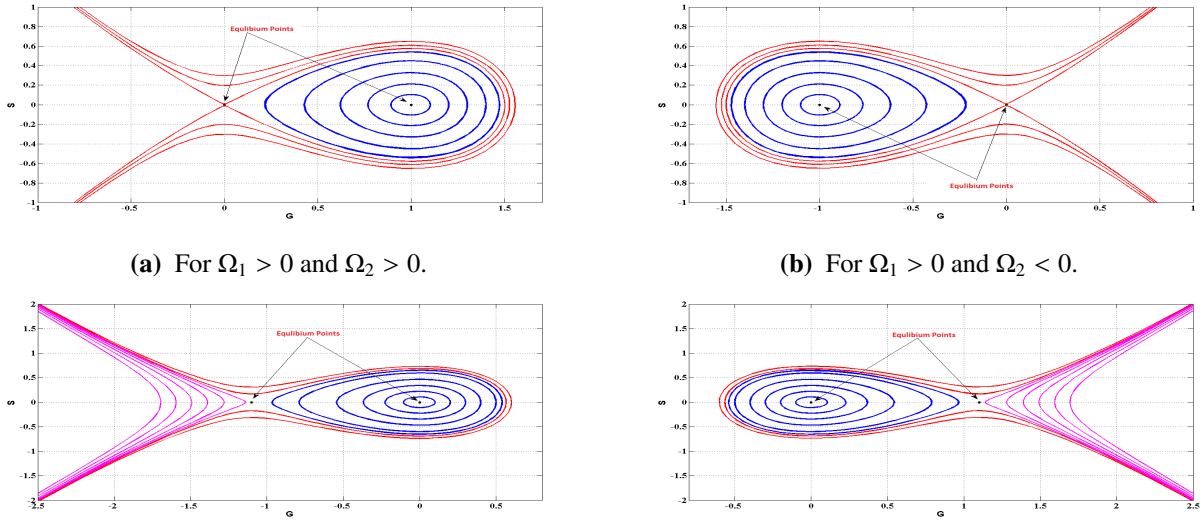

(a) For $\Omega_1 > 0$ and $\Omega_2 > 0$.

(b) For $\Omega_1 > 0$ and $\Omega_2 < 0$.

(c) For $\Omega_1 < 0$ and $\Omega_2 > 0$.

(d) For $\Omega_1 < 0$ and $\Omega_2 < 0$.

Figure 6. Phase portraits for the dynamical system given by Eq (4.1).

5. Hamiltonian dynamics

Through the application of Hamilton's equations of classical mechanics, we have the following system:

$$\frac{dA}{d\iota} = \mathbb{X}(G, S), \ \ \frac{dB}{d\iota} = \mathbb{Y}(G, S). \tag{5.1}$$

The system is generally referred to as Hamiltonian if a function $H(G, S)$ exists such that

$$\mathbb{X} = \frac{\partial H}{\partial S} \ \text{ and } \ \mathbb{Y} = -\frac{\partial H}{\partial G}. \tag{5.2}$$

The Hamiltonian function [39] for the specified system is thus denoted by H.

Definition 1.

The following criteria must be met for the dynamical system given by Eq (5.1) to be Hamiltonian:

$$\frac{\partial \mathbb{X}}{\partial G} + \frac{\partial \mathbb{Y}}{\partial S} = 0.$$

Equation (4.1) is the Hamiltonian dynamical system, according to the definition, since both meet the criteria for the following state equation:

$$\frac{\partial}{\partial G}(\frac{dG}{d\epsilon}) + \frac{\partial}{\partial S}(\frac{dS}{d\epsilon}) = 0.$$

To do this, we write the Hamiltonian function for Eq (4.1) as follows:

$$H(G, S) = \frac{S^2}{2} - \frac{\Omega_1 G^2}{2} + \frac{\Omega_2 G^3}{3}.$$

Definition 2.

Assuming that the equilibrium point of $H(G, S)$ is (G_0, S_0), and that the partial derivatives H_{GG}, H_{SS}, and H_{GS} are continuous on some interval (G_0, S_0), then the following equation holds at this point

$$\Theta(G, S) = H_{GG} \times H_{SS} - (H_{GS})^2.$$

Type 1: When $\Theta(G, S)$ is greater than zero, $\Theta(G, S)$ reaches a either maximum or minimum value at the point (G, S).
Type 2: If $\Theta(G, S)$ is less than zero, $\Theta(G, S)$ exhibits a saddle point at (G, S).
Type 3: When $\Theta(G, S)$ equals zero, various methods are required to determine the nature of the critical point. If the dynamical system's phase can be expressed by the contours of $H(G, S)$, then the center node described in Type 1 will be the equilibrium point at (G, S), and the saddle node in Type 1.

A complete classification is presented in Table 1.

Table 1. Phase portrait classification.

Figure	State Points	$\Theta(G, S)$	Classification
6a	Q_{1a}	-1	Unstable and saddle
6a	Q_{1b}	1	Stable and center
6b	Q_{2a}	-1	Unstable and saddle
6b	Q_{2b}	1	Stable and center
6c	Q_{3a}	1.1	Stable and center
6c	Q_{3b}	-1.1	Unstable and saddle
6d	Q_{4a}	1.1	Stable and center
6d	Q_{4b}	-1.1	Unstable and saddle

6. Quasiperiodic and chaotic patterns

Here, we investigate the potential for quasiperiodic and chaotic behavior in the system described by Eq (4.1) through the introduction of a disturbance. Our analysis involves the study of both two-dimensional and three-dimensional phase diagrams that are specific to this system. We shall delve into the dynamics of the aforementioned system [40]:

$$\begin{cases} \dfrac{dG}{d\epsilon} = S, \\ \dfrac{dS}{d\epsilon} = \Omega_1 G - \Omega_2 G^2 + e_0 \cos(e_1 \epsilon). \end{cases} \tag{6.1}$$

The amplitude is denoted by e_0, while the frequency is denoted by e_1. Upon analyzing the system's sensitivity to the parameter e_1, one can find that the phase diagrams reveal an interesting pattern that highlights the system's susceptibility to variations in the parameter e_1.

Case 1: If $\Omega_1 > 0$ and $\Omega_2 > 0$ with $e_1 = 1$ and $e_1 = 0.09$, the system described by Eq (6.1) exhibits quasi-periodic behavior, as shown in Figures 7a–8c. The statements in the phase diagrams appear as perfectly balanced, repetitive plots, suggesting stable and reliable dynamics.

Case 2: The behavior observed in the nonlinear system in which $\Omega_1 < 0$ and $\Omega_2 > 0$, or $\Omega_1 < 0$ and $\Omega_2 < 0$, with $e_0 = 1.2$ and $e_1 = 3$, governed by Eq (6.1), is of particular significance due to its manifestation of chaotic behavior, as shown in Figures 9a–10c. Chaotic behavior manifests when $e_0 = 1.2$ and $e_1 = 3$.

In this scenario, the system displays non-periodic behavior, instead of exhibiting chaotic characteristics. The trajectories converge and reveal a strong dependence on the initial states of the dynamic processes. The unexpected behavior of this system is solely influenced by the parameter e_1. This behavior comprises fluctuations and chaos that can be observed for different values of e_1, highlighting the complex influence of the perturbed term $e_0 \cos(e_1 \epsilon)$ on the system. The introduction of this perturbation initiates a transition from ordered periodic patterns to chaotic motion, illustrating the intricate interplay of parameters within the system.

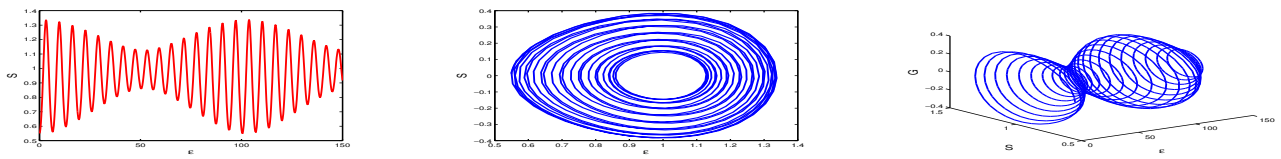

(a) Time series **(b)** 2D quasi-periodic behavior **(c)** 3D quasi-periodic behavior

Figure 7. Phase portraits of the suggested system given by Eq (6.1) are depicted under the condition that $\Omega_1 > 0$, $\Omega_2 > 0$, $e_0 = 0.02$ and $e_1 = 1$.

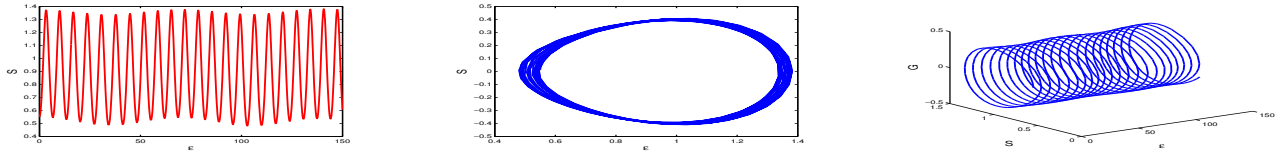

(a) Time series **(b)** 2D quasi-periodic behavior **(c)** 3D quasi-periodic behavior

Figure 8. Phase portraits of the suggested system given by Eq (6.1) are depicted under the condition that $\Omega_1 > 0$, $\Omega_2 > 0, e_0 = 0.02$ and $e_1 = 1$.

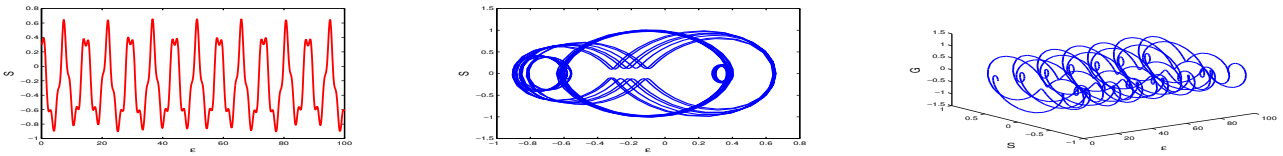

(a) Time series **(b)** 2D chaotic behavior **(c)** 3D chaotic behavior

Figure 9. Phase portraits of the suggested system given by Eq (6.1) are depicted under the condition that $\Omega_1 < 0$, $\Omega_2 > 0, e_0 = 1.2$ and $e_1 = 3$.

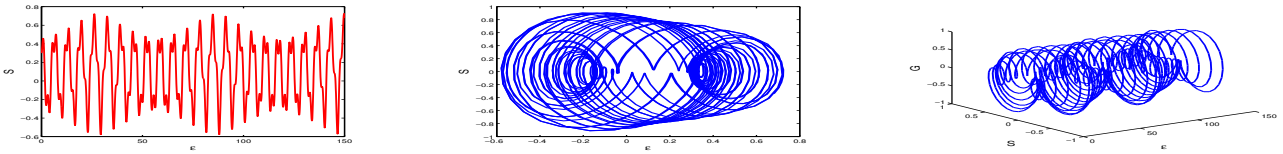

(a) Time series **(b)** 2D chaotic behavior **(c)** 3D chaotic behavior

Figure 10. Phase portraits of the suggested system given by Eq (6.1) are depicted under the condition that $\Omega_1 < 0$, $\Omega_2 < 0, e_0 = 1.2$ and $e_1 = 3$.

7. Lyapunov exponent

The Lyapunov exponent in Figure 11 estimates the rates of increase of distance between initially close trajectories in phase space. A positive index is usually associated with chaos while a negative exponent is associated with stability. A zero index means that stability margins are marginal. The maximum positive influence leads to the occurrence of deterministic patterns, and the changes look random throughout history. Instability, for example, is depicted as orbits that drift or collide, which symbolizes chaos. The Lyapunov exponent has wide-ranging applicability in, engineering, biology, and economics, and it is broadly used for such complex systems as weather patterns and financial markets [41].

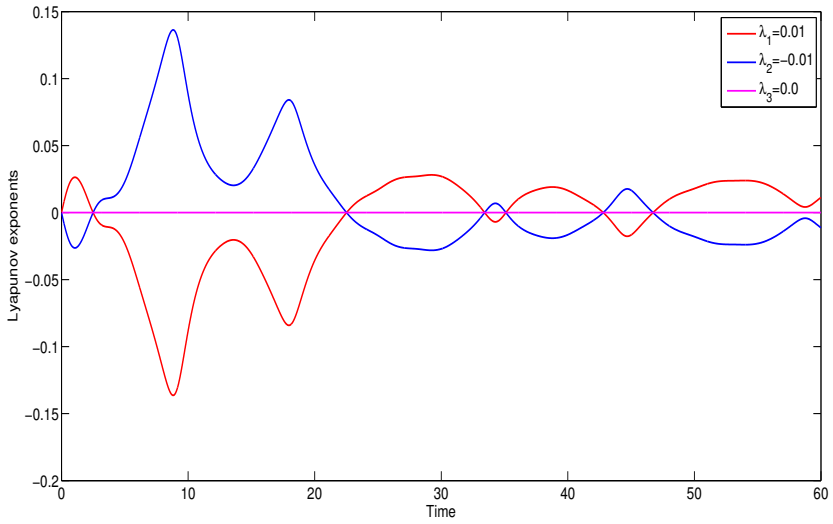

Figure 11. Dynamics of Lyapunov exponents of Eq (4.1).

8. Sensitivity discussion

Sensitivity analysis is an indispensable tool for delineating how changes in inputs or parameters affect the outcome of a system change: as it provides vital information that allows for comprehension of its behavior. A tipping point has been reached in the structural engineering practice, as sensitivity analysis has become a vital tool because of its ability to explore how structural behavior is affected by changes in physical properties or conditions. For our structural engineering model, we consider the sensitivity analysis features that would allow us to track the structure's reliability and understand the effects of changing the material properties or initial conditions on its dynamic response [42]. A detailed analysis is reported in Tables 2 and 3.

Furthermore, the analysis goes beyond just considering how changing the initial conditions affects the overall dynamical structure. Instead, it entails conducting a thorough examination to reveal intricate details regarding the system vectors and mechanisms of response. Through the methodical exploration and examination of this phenomenon, we ultimately aimed to elucidate the intricate interplay between the initial conditions and the dynamic structure's development, broadening our understanding and thus, proffering to the advancement of the structural engineering body of knowledge.

Table 2. Values of parameters utilized in sensitivity analysis.

Figure	Red Curve	Green Curve	Condition
12a	(0.45,0.03)	(0.47,0.04)	$\Omega_1 < 0, \Omega_2 > 0, a < 0$
12b	(0.30,0.03)	(0.35,0.04)	$\Omega_1 > 0, \Omega_2 > 0, a > 0$

Table 3. Values of parameters utilized in sensitivity analysis.

Figure	Red Curve	Green Curve	Blue Curve	Condition
12c	(0.40,0.03)	(0.30,0.04)	(0.35,0.04)	$\Omega_1 < 0, \Omega_2 > 0, a = 0$
12d	(0.40,0.03)	(0.35,0.04)	(0.30,0.04)	$\Omega_1 > 0, \Omega_2 < 0, b < 0$

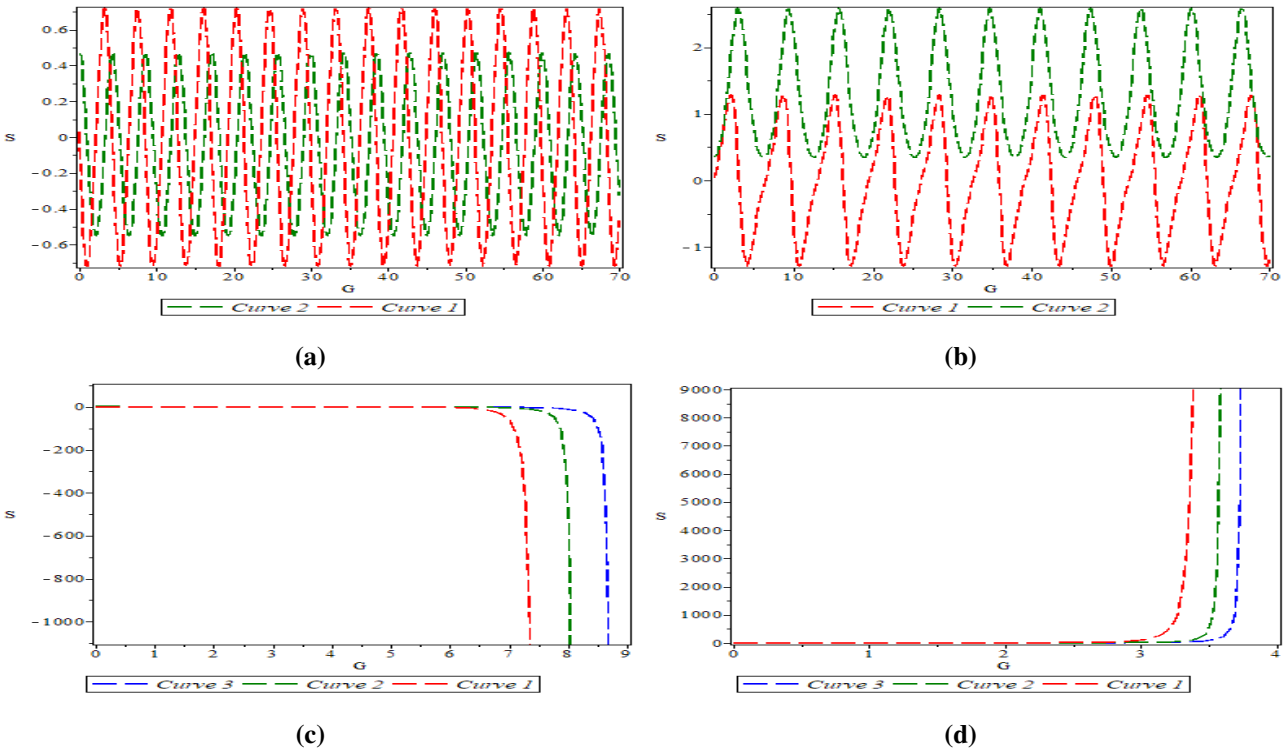

Figure 12. Sensitivity plots generated for the dynamical system given by Eq (4.1) for the parameters and initial conditions listed in Tables 2 and 3.

9. Multistability

A dynamical system may exhibit multiple solutions simultaneously, depending on the specified set of initial parameters and variables. We explored this phenomenon known as multistability distribution in our research [43]. The methodologies involved analyzing phase portraits and time series graphs to understand various multistability behaviors of the system given by Eq (4.1).

To test our software function, we set specific parameter values: $a = 0.1$, $b = -1$, $c = 1$, $k = 1$, $e_0 = 1.2$, and $e_1 = 3$, as depicted in Figure 13. These plots illustrate the phase portrait results corresponding to the initial conditions $(G, S) = (0.10, 0.01)$, shown in red, $(G, S) = (0.20, 0.01)$, shown in blue, and $(G, S) = (0.40, 0.01)$, shown in pink. Initially, the tested system exhibited chaotic or periodic behavior.

Figure 14 shows the results of utilizing $a = 2$, $b = 1$, $c = 1$, $k = 1$, $e_0 = 1.2$, and $e_1 = 3$, two distinct phase portraits were generated in red and green for the initial conditions $(R, G) = (0.04, 0.1)$ and $(R, G) = (0.01, 0.1)$, respectively by using unique parameter values. The system exhibited a quasi-periodic behavior for these initial values.

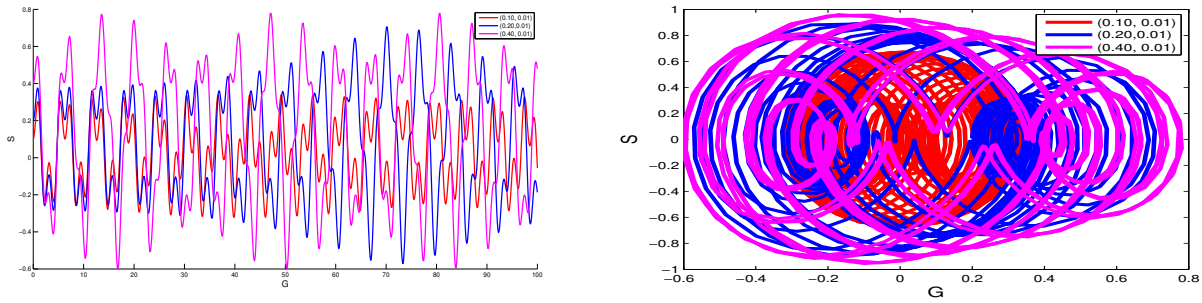

(a) **(b)**

Figure 13. Multistability of the nonlinear dynamical system given by Eq (4.1) with $\Omega_1 < 0$, and $\Omega_2 < 0$.

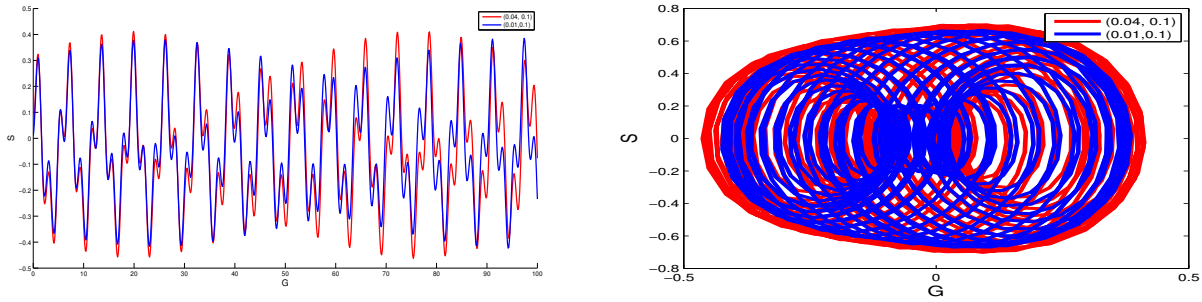

(a) **(b)**

Figure 14. Multistability of the nonlinear dynamical system given by Eq (4.1) with $\Omega_1 < 0$, and $\Omega_2 > 0$.

10. Conservation laws

Conservation laws hold a crucial role in the examination of dynamic systems and have diverse applications across different disciplines. They are generally employed to describe essential physical properties of PDEs that represent various phenomena. These laws are utilized in practical scenarios to identify the integrability and linearization of PDEs, determine first integrals for ordinary differential equations, locate potentials, construct non-locally connected systems, and evaluate the precision of numerically calculated solutions. Consider the following equation:

$$\mathfrak{B}[Q] = \frac{\partial^4 Q}{\partial \iota^2\, \partial \varpi^2} - a\frac{\partial^2 Q}{\partial \iota^2} + \frac{\partial^2 Q}{\partial \varpi^2} + 2b\Big[(\frac{\partial Q}{\partial \iota})^2 + Q\frac{\partial^2 Q}{\partial \iota^2}\Big] = 0. \tag{10.1}$$

The objective was to establish a local conservation law of the divergence type for Eq (10.1) in the following form:

$$D_j\Psi^j[Q] = D_1\Psi^1[Q] + D_2\Psi^2[Q] = 0.$$

For the derived solutions of Eq (10.1), only total derivative operators were considered, resulting in the inclusion of a conservation law multiplier $\mu[Q] = \mu(\varpi, \iota, Q)$ that satisfies

$$\mu[H]\mathfrak{B}[Q] = D_j\Psi^j[H].$$

Here, ψ represents an arbitrary variable without any specific constraints or limitations.

Theorem 5.

Considering the expression of divergence $D_j\psi^j[Q]$, the following equality is valid [44]:

$$E_Q(D_j\psi^j[Q]) = 0,$$

where E_Q shows the Euler operator that is,

$$E_Q = \frac{\partial}{\partial Q} - D_j\frac{\partial}{\partial Q_j} + D_{ji}\frac{\partial}{\partial Q_{ji}} - D_{jik}\frac{\partial}{\partial Q_{jik}} + ... + (-1)^p D_{j_1}...D_{j_p}\frac{\partial}{\partial Q_{j_1....j_p}}.$$

Theorem 6.

If a conservation law multiplier $\mu(\varpi, \iota)$ is available, then it is possible to derive a divergence expression for Eq (10.1):

$$E_Q(\mu(\varpi, \iota))\mathfrak{B}[Q] = 0. \tag{10.2}$$

Theorem 7.

When considering the arbitrary constants a and b, Eq (10.1) allows for the existence of local conservation laws:

$$\begin{cases} D_\varpi(Q_\varpi) + D_\iota(2bQQ_\iota + Q_{\iota\varpi\varpi}) = 0, \\ D_\varpi(\varpi Q_\varpi - Q) + D_\iota(2b\varpi QQ_\iota - a\varpi Q_\iota + \varpi Q_{\varpi\varpi\iota}) = 0, \\ D_\varpi(\iota Q_\varpi) + D_\iota(2b\iota QQ_\iota - a\iota Q_\iota - bQ^2 + aQ + \iota Q_{\iota\varpi\varpi} - Q_{\varpi\varpi}) = 0, \\ D_\varpi(\iota\varpi Q_\varpi - \iota Q) + D_\iota(2b\iota\varpi QQ_\iota - a\iota\varpi Q_\iota - b\varpi Q^2 + a\varpi Q + \iota\varpi Q_{\iota\varpi\varpi} - \varpi Q_{\varpi\varpi}) = 0. \end{cases}$$

The complete set of local conservation laws for Eq (1.3) with constants a and b can be established as $\{\mu_1, \mu_2, \mu_3, \mu_4\} = \{1, \varpi, \iota, \varpi\iota\}$. These conservation law multipliers apply to the entirety of the local conservation laws for the given equation.

Proof. By utilizing the information presented in Eq (10.2), we can deduce the system of equations $\mu_\iota = 0$, $\mu_{\varpi\varpi} = 0$, $\mu_Q = 0$. Subsequently, the following solution can be obtained:

$$\mu = r_1 + r_2\varpi + \iota(r_3 + r_4\varpi). \tag{10.3}$$

The constants denoted by r_j (where $j = 1, 2, 3, 4$) are arbitrary in nature. The solution given by Eq (10.3) allows for a subsequent demonstration that Theorem 7 holds true when the set of conservation law multipliers $\{\mu_1, \mu_2, \mu_3, \mu_4\}$ is defined as $\{1, \varpi, \iota, \varpi\iota\}$ respectively.

11. Conclusions

This paper details an analysis of the Lonngren wave equation within the field of semiconductor physics through the use of Lie symmetry analysis to address its complexities. Through the computation of Lie point symmetries and the identification of one-dimensional conjugacy classes, we have designed an approach for the reduction of the model and find new wave solutions. We applied the tanh technique, which applies to all of the analytical solutions that contain logarithmic and exponential functions.

Moreover, applying the Galilean transformation allowed us to project the equation onto a spatial dynamical system, pinpoint the equilibrium points, and investigate the chaos phenomena via sensitivity analysis. Numerical simulation results indicate that the model is highly sensitive to changes in the frequency and intensity of the perturbation. Lastly, we have presented a complete set of local conservation laws and employed a graphical analysis system to illustrate the variation in nonlinear equation solutions, which has afforded a deep understanding of the problem.

Author contributions

Writing original draft, M.B.R., M.I., and B; Writing review and editing, A.J., A. R. A., M.B.R., M.I., and B.; Methodology, M.B.R., A.J., A. R. A.; Software, M.I., B, and A. R. A.; Supervision, M.B.R., and A.J.; Project administration, A.J., and M.I.; Visualization, A.J., B, and M.B.R.; Conceptualization, A.J., M.B.R., M.I. and A. R. A.; Formal analysis, A.J., A. R. A., B, M.I., and M.B.R.

Use of AI tools declaration

The authors declare they have not used Artificial Intelligence (AI) tools in the creation of this article.

Acknowledgments

This article has been produced with the financial support of the European Union under the REFRESH–Research Excellence For Region Sustainability and High-tech Industries project number CZ .10.03.01/00/22_003/0000048 via the Operational Programme Just Transition.

This project has been partially supported by Gulf University for Science and Technology and the Centre for Applied Mathematics and Bioinformatics under project code: ISG–63.

Conflict of interest

All authors declare that there are no competing interests.

References

1. K. Lonngren, D. Landt, C. Burde, J. Kolosick, Observation of shocks on a nonlinear dispersive transmission line, *IEEE Trans. Circuits Syst.*, **22** (1975), 376–378. https://doi.org/10.1109/TCS.1975.1084039
2. R. Zhang, M. Shakeel, N. B. Turki, N. A. Shah, S. M. Tag, A novel analytical technique for a mathematical model representing communication signals: a new traveling wave solutions, *Results Phys.*, **51** (2023), 106576. https://doi.org/10.1016/j.rinp.2023.106576
3. K. Lonngren, H. C. S. Hsuan, W. F. Ames, On the soliton, invariant, and shock solutions of a fourth-order nonlinear equation, *J. Math. Anal. Appl.*, **52** (1975), 538–545. https://doi.org/10.1016/0022-247X(75)90078-5

4. M. M. Rahman, A. Akhtar, K. C. Roy, Analytical solutions of nonlinear coupled Schrödinger–KdV equation via advanced exponential expansion, *Amer. J. Math. Comput. Model.*, **3** (2019), 46–51. https://doi.org/10.11648/j.ajmcm.20180303.11
5. Ş. Akçaği, T. Aydemir, Comparison between the $(\frac{G'}{G})$-expansion method and the modified extended tanh method, *Open Phys.*, **14** (2016), 88–94. https://doi.org/10.1515/phys-2016-0006
6. H. M. Baskonus, H. Bulut, T. A. Sulaiman, New complex hyperbolic structures to the lonngren-wave equation by using sine-gordon expansion method, *Appl. Math. Nonlinear Sci.*, **4** (2019), 129–138. https://doi.org/10.2478/AMNS.2019.1.00013
7. S. Duran, Breaking theory of solitary waves for the Riemann wave equation in fluid dynamics, *Int. J. Modern Phys. B*, **35** (2021), 2150130. https://doi.org/10.1142/S0217979221501307
8. I. Aziz, I. Khan, Numerical solution of diffusion and reaction-diffusion partial integrodifferential equations, *Int. J. Comput. Methods*, **15** (2018), 1850047. https://doi.org/10.1142/S0219876218500470
9. W. Gao, H. M. Baskonus, L. Shi, New investigation of bats-hosts-reservoir-people coronavirus model and application to 2019-nCoV system, *Adv. Differ. Equ.*, **2020** (2020), 391. https://doi.org/10.1186/s13662-020-02831-6
10. K. K. Ali, R. Yilmazer, A. Yokus, H. Bulut, Analytical solutions for the (3+1)-dimensional nonlinear extended quantum Zakharov–Kuznetsov equation in plasma physics, *Phys. A: Stat. Mechanics Appl.*, **548** (2020), 124327. https://doi.org/10.1016/j.physa.2020.124327
11. H. M. Baskonus, H. Bulut, On the complex structures of Kundu-Eckhaus equation via improved Bernoulli sub-equation function method, *Waves Random Complex Media*, **25** (2015), 720–728. https://doi.org/10.1080/17455030.2015.1080392
12. B. Dünweg, U. D. Schiller, A. J. Ladd, Statistical mechanics of the fluctuating lattice Boltzmann equation, *Phys. Rev. E*, **76** (2007), 036704. https://doi.org/10.1103/PhysRevE.76.036704
13. W. X. Ma, Z. Zhu, Solving the (3+1)-dimensional generalized KP and BKP equations by the multiple exp-function algorithm, *Appl. Math. Comput.*, **15** (2012), 11871–11879. https://doi.org/10.1016/j.amc.2012.05.049
14. A. R. Seadawy, Traveling-wave solutions of a weakly nonlinear two-dimensional higher-order Kadomtsev-Petviashvili dynamical equation for dispersive shallow-water waves, *Eur. Phys. J. Plus*, **132** (2017), 29. https://doi.org/10.1140/epjp/i2017-11313-4
15. S. F. Tian, M. J. Xu, T. T. Zhang, A symmetry-preserving difference scheme and analytical solutions of a generalized higher-order beam equation, *Proc. Roy. Soc. A*, **477** (2021), 20210455. https://doi.org/10.1098/rspa.2021.0455
16. J. S. Russell, *Report on waves: made to the meetings of the British Association in 1842-43*, London: Printed by Richard and John E. Taylor, 1845.
17. P. G. Drazin, R. S. Johnson, *Solitons: an introduction*, 2 Eds, Cambridge University Press, 1989. https://doi.org/10.1017/CBO9781139172059
18. X. B. Wang, S. F. Tian, C. Y. Qin, T. T. Zhang, Lie symmetry analysis, conservation laws, and analytical solutions of a time-fractional generalized kdv-type equation, *J. Nonlinear Math. Phys.*, **24** (2017), 516–530. https://doi.org/10.1080/14029251.2017.1375688

19. A. Jhangeer, A. R. Ansari, M. Imran, Beenish, M. B. Riaz, Conserved quantities and sensitivity analysis the influence of damping effect in ferrites materials, *Alex. Eng. J.*, **86** (2024), 298–310. https://doi.org/10.1016/j.aej.2023.11.067

20. M. Wang, X. Li, Applications of f-expansion to periodic wave solutions for a new Hamiltonian amplitude equation, *Chaos, Soliton. Fract.*, **24** (2005), 1257–1268. https://doi.org/10.1016/j.chaos.2004.09.044

21. F. González-Gascón, A. González-López, Symmetries of differential equations. IV, *J. Math. Phys.*, **24** (1983), 2006–2021. https://doi.org/10.1063/1.525960

22. E. Fan, Extended tanh-function method and its applications to nonlinear equations, *Phys. Lett. A*, **277** (2000), 212–218. https://doi.org/10.1016/S0375-9601(00)00725-8

23. S. San, R. Altunay, Application of the generalized Kudryashov method to various physical models, *Appl. Math. I Infor. Sci. Lett.*, **8** (2021), 7–13.

24. A. M. Wazwaz, The tanh and the sine-cosine methods for the complex modified K dv and the generalized K dv equations, *Comput. Math. Appl.*, **49** (2005), 1101–1112. https://doi.org/10.1016/j.camwa.2004.08.013

25. S. San, R. Altunay, Abundant traveling wave solutions of (3+1) dimensional Boussinesq equation with dual dispersion, *Rev. Mex. Fís. E*, **19** (2022), 020203. https://doi.org/10.31349/RevMexFisE.19.020203

26. M. M. A. Khater, D. Kumar, New exact solutions for the time fractional coupled Boussinesq–Burger equation and approximate long water wave equation in shallow water, *J. Ocean Eng. Sci.*, **2** (2017), 223–228. https://doi.org/10.1016/j.joes.2017.07.001

27. A. Jhangeer, N. Raza, H. Rezazadeh, A. Seadawy, Nonlinear self-adjointness, conserved quantities, bifurcation analysis and traveling wave solutions of a family of long-wave unstable lubrication model, *Pramana*, **94** (2020), 87. https://doi.org/10.1007/s12043-020-01961-6

28. A. Hussain, M. Usman, B. R. Al-Sinan, W. M. Osman, T. F. Ibrahim, Symmetry analysis and closed-form invariant solutions of the nonlinear wave equations in elasticity using an optimal system of Lie sub-algebra, *Chinese J. Phys.*, **83** (2023), 1–13. https://doi.org/10.1016/j.cjph.2023.02.011

29. V. A. Dorodnitsyn, E. I. Kaptsov, R. V. Kozlov, S. V. Meleshko, One-dimensional MHD flows with cylindrical symmetry: Lie symmetries and conservation laws, *Int. J. Nonlinear Mech.*, **148** (2023), 104290. https://doi.org/10.1016/j.ijnonlinmec.2022.104290

30. A. Abdallah, I. Abbas, H. Sapoor, The effects of fractional derivatives of bioheat model in living tissues using the analytical-numerical method, *Infor. Sci. Lett.*, **11** (2022), 7–13. http://doi.org/10.18576/isl/110102

31. L. Zada, M. Al-Hamami, R. Nawaz, S. Jehanzeb, A. Morsy, A. Abdel-Aty, et al., A new approach for solving Fredholm integro-differential equations, *Infor. Sci. Lett.*, **10** (2021), 407–415. http://doi.org/10.18576/isl/100303

32. L. Akinyemi, A fractional analysis of Noyes-Field model for the nonlinear Belousov-Zhabotinsky reaction, *Comput. Appl. Math.*, **39** (2020), 175. http://doi.org/10.1007/s40314-020-01212-9

33. L. T. K. Nguyen, Soliton solution of good Boussinesq equation, *Vietnam J. Math.*, **44** (2016), 375–385. https://doi.org/10.1007/s10013-015-0157-8

34. L. T. K. Nguyen, N. F. Smyth, Modulation theory for radially symmetric kink waves governed by a multi-dimensional Sine-Gordon equation, *J. Nonlinear Sci.*, **33** (2023), 11. https://doi.org/10.1007/s00332-022-09859-w

35. H. Almusawa, A. Jhangeer, Beenish, Soliton solutions, lie symmetry analysis and conservation laws of ionic waves traveling through microtubules in live cells, *Results Phys.*, **43** (2022), 106028. https://doi.org/10.1016/j.rinp.2022.106028

36. S. San, A. Akbulut, Ö. Ünsal, F. Taşcan, Conservation laws and double reduction of (2+1) dimensional Calogero–Bogoyavlenskii–Schiff equation, *Math. Methods Appl. Sci.*, **40** (2017), 1703–1710. https://doi.org/10.1002/mma.4091

37. P. J. Olver, *Applications of Lie groups to differential equations*, Springer Science & Business Media, Vol. 107, 1993.

38. Beenish, H. Kurkcu, M. B. Riaz, M. Imran, A. Jhangeer, Lie analysis and nonlinear propagating waves of the (3+1)-dimensional generalized Boiti–Leon–Manna–Pempinelli equation, *Alex. Eng. J.*, **80** (2023), 475–486. https://doi.org/10.1016/j.aej.2023.08.067

39. R. Grimshaw, *Nonlinear ordinary differential equations,* Routledge, 2017. https://doi.org/10.1201/9780203745489

40. A. Jhangeer, Beenish, Study of magnetic fields using dynamical patterns and sensitivity analysis, *Chaos, Soliton. Fract.*, **182** (2024), 114827. https://doi.org/10.1016/j.chaos.2024.114827

41. S. Banerjee, M. K. Hassan, S. Mukherjee, A. Gowrisankar, *Fractal patterns in nonlinear dynamics and applications,* CRC Press, 2020. https://doi.org/10.1201/9781315151564

42. K. K. Ali, W. A. Faridi, A. Yusuf, M. Abd El-Rahman, M. R. Ali, Bifurcation analysis, chaotic structures and wave propagation for nonlinear system arising in oceanography, *Results Phys.*, **57** (2024), 107336. https://doi.org/10.1016/j.rinp.2024.107336

43. H. Natiq, S. Banerjee, A. P. Misra, M. R. Said, Degenerating the butterfly attractor in a plasma perturbation model using nonlinear controllers, *Chaos, Soliton. Fract.*, **122** (2019), 58–68. https://doi.org/10.1016/j.chaos.2019.03.009

44. R. Naz, Conservation laws for some compaction equations using the multiplier approach, *Appl. Math. Lett.*, **25** (2012), 257–261. https://doi.org/10.1016/j.aml.2011.08.019

AIMS Press